How are heat waves over Yangtze River valley associated with atmospheric quasi-biweekly oscillation?

Miaoni Gao, Jing Yang, Bin Wang, Siyuan Zhou, Daoyi Gong & Seong-Joong Kim

Climate Dynamics
Observational, Theoretical and Computational Research on the Climate System

ISSN 0930-7575

Clim Dyn
DOI 10.1007/s00382-017-3526-z

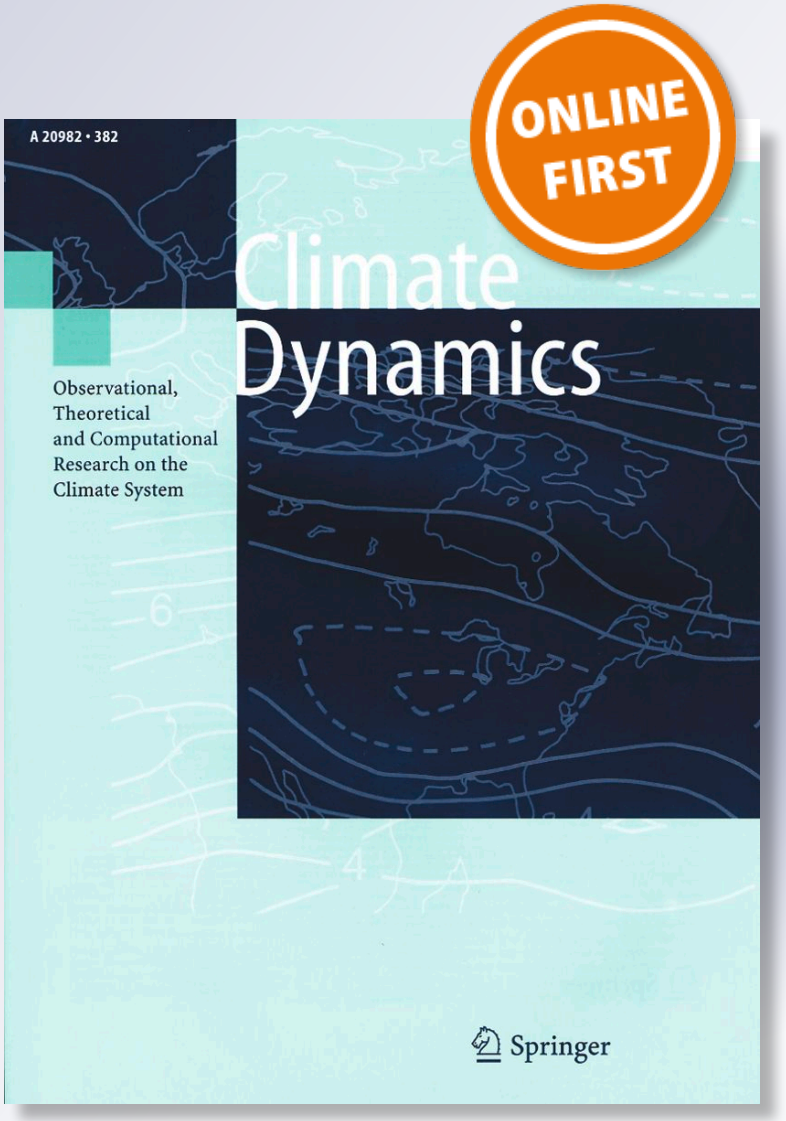

Springer

Clim Dyn
DOI 10.1007/s00382-017-3526-z

How are heat waves over Yangtze River valley associated with atmospheric quasi-biweekly oscillation?

Miaoni Gao[1,2,3] · Jing Yang[1,2] · Bin Wang[3,4] · Siyuan Zhou[2] · Daoyi Gong[1,2] · Seong-Joong Kim[5]

Received: 23 July 2016 / Accepted: 8 January 2017

Abstract Over Yangtze River valley (YRV) where heat wave (HW) events most frequently occur in China during 1979–2014, 30 out of 57 HW events (nearly 55%) in July and August is found to be related with the dry phases of atmospheric quasi-biweekly oscillation (QBWO). When a significant low-level anticyclonic anomaly (LAA) associated with QBWO appears over YRV, temperature rises sharply according to the adiabatic heating caused by subsidence and the enhanced downward solar radiation due to decreased clouds. The LAA with subsidence over YRV is primarily generated by quasi-biweekly atmospheric waves, which are classified to three types through case-by-case categorization, named as "mid-latitude wavetrain", "WNP (western North Pacific) wavetrain" and "double wavetrains", respectively. The mid-latitude wavetrain QBWO causes the LAA through subsidence induced by upper-level cyclonic vorticity which is associated with an eastward/southeastward migrating wave train from Eastern Europe to WNP in the upper troposphere. The WNP wavetrain QBWO forms LAA through a northwestward migrating lower-tropospheric wave train emanating from tropical WNP to southeastern China. The double wavetrains QBWO triggers LAA through both the low-level shear anticyclonic vorticity provided by a low-level northwestward/westward propagating wave train from tropical WNP to South China Sea and the upper-level positive vorticity associated with an eastward/southeastward migrating wave train from Eastern Europe to southeastern China in the upper troposphere. In all cases, South Asian High extends eastward and WNP subtropical high extends westward during HW events. Tracing these distinct precursory circulation anomalies may facilitate better understanding and short-medium range forecast of HW.

Keywords Heat wave · Yangtze River valley · Quasi-biweekly oscillation · Wave trains

✉ Jing Yang
yangjing@bnu.edu.cn

1 State Key Laboratory of Earth Surface Processes and Resource Ecology (ESPRE), Faculty of Geographical Science, Beijing Normal University, Beijing 100875, China

2 Academy of Disaster Reduction and Emergency Management, Faculty of Geographical Science, Beijing Normal University, Beijing 100875, China

3 Department of Meteorology, and International Pacific Research Center, University of Hawaii at Manoa, Honolulu 96822, HI, USA

4 Earth System Modeling Center, Nanjing University of Information Science and Technology, Nanjing 210044, China

5 Division of Climate Change, Korea Polar Research Institute, Incheon, South Korea

1 Introduction

Heat wave (HW) brings severe impacts on society, economy, biology and human health (e.g., Easterling et al. 2000). In the past half centuries, HW occurrence increased in Asia (Hartmann et al. 2013). In 2013, China has suffered a super summertime HW with unprecedented spatial extent, duration and high temperature (Peng 2014). Understanding the underlying causes and improving the HW forecast is crucial for disaster reduction. Most studies concentrated on the linkage between large-scale background and HW including western North Pacific (WNP) subtropical high (WNPSH) (e.g., Peng 2014), South Asian High (e.g., Liu et al. 2006), North Atlantic Oscillation (Sun 2012), vortex (Zhang et al. 2005) and sea surface temperature (Lei et al.

Published online: 07 February 2017

2009; Sun 2014). However, the mechanism of short-range HW occurrence is still not fully understood.

As will be shown in Sect. 3, the atmospheric circulation over the Yangtze River valley (YRV) exhibits significant quasi-biweekly oscillation (QBWO). According to previous studies, atmospheric QBWO is one of the dominant intraseasonal variation (ISV) modes in boreal summer over this region (e.g., Mao and Wu 2006; Yang et al. 2010; Chen et al. 2015). Many studies have found the noticeable contribution of QBWO wet phase to extreme rainfall events over YRV (e.g., Chan et al. 2002; Liu et al. 2014). Here, we subsequently speculate if the QBWO dry phase could influence the extreme dry events such as HW. Actually, several studies have detected the impact of ISV on HW occurrence (Ding and Qian 2012; Teng et al. 2013). Teng et al. (2013) found that many US HW events were related with an anticyclonic circulation due to the energy propagation of a striking zonal wavenumber-5 Rossby wave train found 15 days in advance, which resembled the leading pattern of subseasonal variability in nature. According to statistics of 87 dry HW events over southern China during 1979–2008, Ding and Qian (2012) proposed that HW events had close relationship between upper-level regional-scale geopotential height anomalies from Europe or WNP which appeared 7 days before HW on the average. However, both studies focused on the intraseasonal precursors of HW events based on statistical analyses of geopotential height. Less attention was paid to the detailed ISV evolution and their influence on the genesis of extremely high temperature during HW.

The present study investigates the characteristics and genesis of the QBWO-associated HW events. The paper is composed of as follows. A brief description of the datasets and methods is given in the next section. Section 3 shows the definitions, key region, dominant periodicity and the cases of HW that we selected over China. In Sect. 4, common features of HW, QBWO dry phase and the local genesis of extremely high temperature are diagnosed. In Sect. 5, different behaviors and evolutions of the QBWO are identified with three types of HW events. The final section is conclusion and discussion.

2 Datasets and methodology

2.1 Datasets

The newly released CN05.1 dataset from the National Climate Center in China with a high spatial resolution (0.25°) for the period of 1979–2014 was used to depict the HW events, including daily maximum temperature (T_{max}), daily minimum temperature (T_{min}), daily mean 2 m temperature (T_m), precipitation and relative humidity (Xu et al. 2009; Wu and Gao 2013). The daily atmospheric circulation, temperature, radiative fluxes and cloud cover used in this study were extracted from the ERA-interim reanalysis datasets with a 1° spatial resolution and 37 pressure levels in the vertical direction for the period of 1979–2014 produced by the European Centre for Medium-range weather forecasts (Dee et al. 2011). Cloud cover based on ERA-interim dataset was compared with that from Moderate Resolution Imaging Spectroradiometer (MODIS) dataset provided by National Aeronautics and Space Administration (NASA) for cross validation (Levy et al. 2015). Although the MODIS dataset only covers the period after 2002, the above two cloud datasets produce similar results.

2.2 Methodology

2.2.1 The ISV extraction and significance test

The ISV component was obtained from the "raw" daily time series through first removing the slow annual cycle (climatology and the first three Fourier harmonics) and then removing synoptic fluctuations by taking a 5-day running mean (Yang et al. 2010).

To identify the dominant QBWO periodicity, power spectrum analysis through FFT with a tapered window (Bingham et al. 1967) was applied to the time series of ISV component over the core region during July to August each year. Then the average of individual power spectrum for the 36 summers (1979–2014) was calculated with significance test (Gilman et al. 1963). Based on the results of spectrum analysis, an 8-21-day band-filtering was applied on the ISV component based on fast Fourier transform (FFT) to derive the QBWO component (Bloomfield 2000).

In order to describe the structure and behavior of QBWO, each cycle of the selected QBWO events was separated into eight phases. Phase 1 is the maximum (peak wet phase) and phase 5 is the minimum (peak dry phase). Phases 3 and 7 are the transitions from wet to dry phase and from dry to wet phase, respectively. Phases 2, 4, 6 and 8 occur at the times when the cycle reaches half of its maximum or minimum. Then QBWO-associated HW events were classified into different types through case-by-case categorization. And phase compositing technique (e.g., Fujinami and Yasunari 2004; Yang et al. 2014) was used to perform composite analysis of each type of HW events with common features based on their individual life cycle.

The Theil-Sen trend estimation method (Gilbert 1987) and the Mann–Kendall trend significance test (Kendall 1975) were applied to extract the linear trend of the HW frequency over the core region during the period of 1979–2014.

2.2.2 Temperature budget diagnosis

Temperature budget equation was used to understand temperature changes associated with atmospheric QBWO during the HW events. According to Yanai et al. (1973), the temperature tendency at each constant level is determined by the combined effects of the horizontal temperature advection, the adiabatic process related to vertical motion and the atmospheric apparent heat source (Q_1). The equation could be written as $\frac{\partial T}{\partial t} = -V \times \nabla T + \omega\sigma + \frac{Q_1}{c_p}$, where c_p denotes the specific heat at constant pressure, T the temperature, t the time, V the horizontal velocity vector, ∇ the horizontal gradient operator, p the pressure, ω the vertical p velocity, $\sigma = \left(RT/c_p p\right) - (\partial T/\partial p)$ the static stability and R the gas constant. In addition, Q_1 includes the radiative heating, latent heating, surface heat flux and subgrid-scale processes. Therefore, the radiative fluxes at surface were further diagnosed. To derive the QBWO component of this equation, we applied 8–21-day filtering operator to each term of the equation (Zhao et al. 2013). Note that the temperature tendency was calculated by the centered finite difference method.

2.2.3 Wave-activity flux

To illustrate the wave energy propagation, a phase-independent wave-activity flux formulated by Takaya and Nakamura (2001) was calculated, which has been used in previous studies of mid-latitude wave train on the intraseaonal timescale (e.g., Yang and Li 2016). The equation could be expressed as: $W = \frac{1}{|\bar{U}|}\begin{bmatrix} \bar{u}(\psi_x'^2 - \psi'\psi_{xx}') + \bar{v}(\psi_x'\psi_y' - \psi'\psi_{xy}') \\ \bar{u}(\psi_x'\psi_y' - \psi'\psi_{xy}') + \bar{v}(\psi_x'^2 - \psi'\psi_{yy}') \end{bmatrix}$, where W represents the horizontal wave-activity flux, U the wind velocity, u and v the zonal and meridional wind, ψ the stream function and a bar and a prime the low-frequency background state component (greater than 21 days) and QBWO component, respectively.

3 HW events over the Yangtze River valley

3.1 Definitions of HW in China

Several reasonable indices have been proposed to recognize HW events through setting a local threshold temperature in a certain region (e.g., Steadman 1984; Qian and Lin 2004; Anderson and Bell 2011; Smith et al. 2013). The HW indices can be generally divided into two main groups according to the type of threshold used when defining HW: the absolute thresholds (e.g., Robinson 2001; Huang et al. 2010; Ding and Qian 2011) and the relative thresholds which are designed to eliminate the regional diversities (percentile threshold approach) (e.g., Liu et al. 2008; Anderson and Bell 2011). Since China has diverse graphic and climate characteristics due to the vast territory, both absolute and relative criteria were applied to identify HW events for each grid in China to obtain more reliable results.

In this study, we used five criteria to identify one HW event at each grid in order to obtain the core region of HW events in China: a HW event is defined as equal or more than (I) 3 succeeding days with T_{max} exceeding 35 °C (Huang et al. 2010); (II) 2 succeeding days with T_{max} exceeding 35 °C and T_{min} exceeding 26.7 °C (Ding and Qian 2011); (III) 2 succeeding days with daily maximum HW index exceeding 40.6 °C and daily minimum HW index exceeding 26.7 °C (Robinson 2001); (IV) 3 succeeding days with T_{max} exceeding 90th percentile of the climatology (Liu et al. 2008); (V) 2 succeeding days with T_m exceeding 95th percentile of the climatology (Anderson and Bell 2011). Among five HW definitions, I–III are absolute criteria and IV–V are percentile criteria. Compared with criterion I and IV which only use T_{max} as the indicator, criterion II, III and V have taken T_{min} into consideration.

For selecting regional HW events, we used two definitions containing not only T_{max} but also T_{min} in light of the consecutive nights with warm nighttime temperature have important impacts on human health (Meehl and Tebaldi 2004; Gershunov et al. 2009). The first HW definition is a relative definition, in which a HW event refers to a spell of at least 4 consecutive days with core region averaged T_m exceeding the local 90th percentile of the period with a 15-day running mean to remove the synoptic fluctuations (Gong et al. 2004; Teng et al. 2013, with modified). The second one is the absolute definition proposed by Robinson (2001) aforementioned.

3.2 The core region of HW in China during July and August

According to Wang et al. (2009), the climatology over East Asia shows distinct features between May–June and July–August (called as JA for short) because the rainy zone shifts to north of the Yangtze River after July. After the Meiyu front migrates northward, YRV is under the influence of WNPSH which favors for the local high temperature in JA. Previous studies have pointed out that JA is the peak season of HW events with high humidity over southeastern China (Hu et al. 2012; Ding and Ke 2015). Therefore, we focused on JA in our analysis.

Figure 1 displays the frequency of HW occurrence over China in 36 summers based on the aforementioned five HW definitions for each grid. Their common results exhibit that YRV is the salient center of HW frequency in China, where

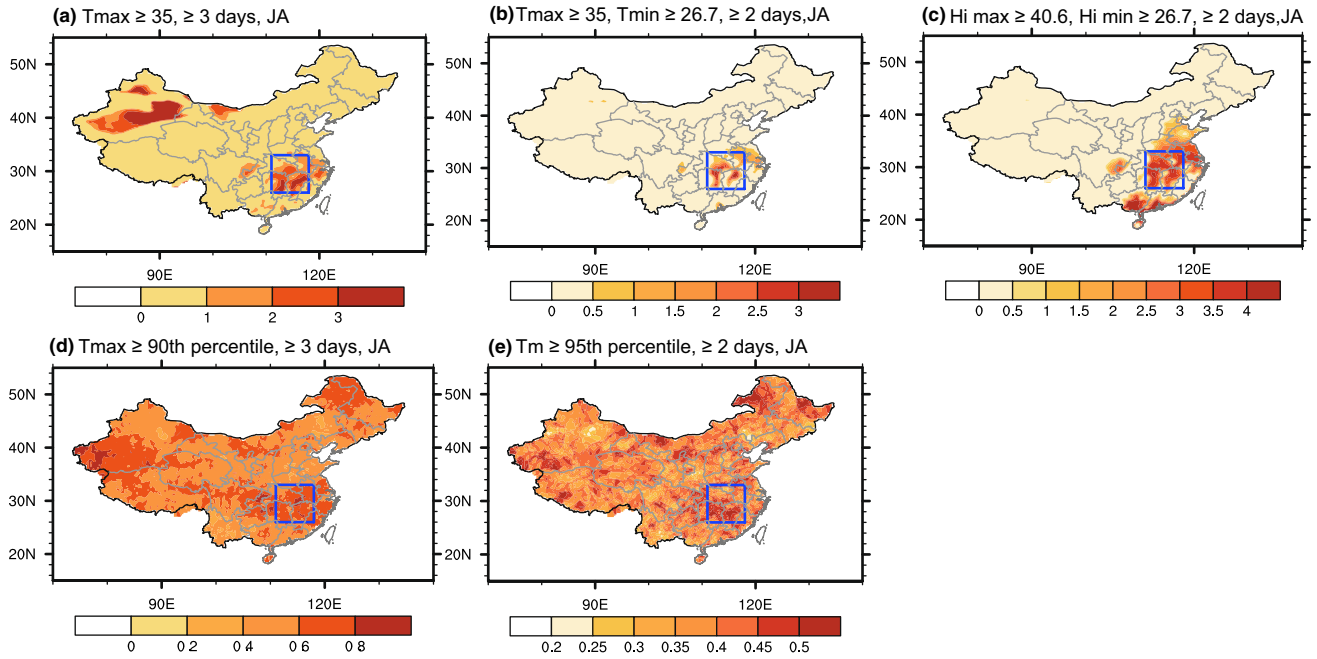

Fig. 1 The frequency of HW occurrence over YRV (times/year) in JA derived from the CN05.1 dataset during 1979–2014. The HW frequency is calculated based on the criterion **a** I, **b** II, **c** III, **d** IV and **e** V, respectively. The *blue box* is the YRV core region

the averaged maximum frequency based on five criteria exceeds 2.3 times/year. The HW events there are characterized by both the high temperature and high humidity. Thus, YRV (26°–33°N, 111°–118°E) is defined as the core region of China HW events in this study.

3.3 Selection of regional HW events associated with significant QBWO cases

The next step is to choose the HW events over the YRV core region. Total 64 HW events are identified according to the relative regional HW definition and 111 HW events are recognized according to the absolute definition (Fig. 2). To obtain reliable results, 57 HW cases that satisfied both definitions were finally chosen in the following study.

To obtain the dominant periodicity of the atmospheric circulation over YRV, we analyzed power spectrum of the region-averaged precipitation and T_m for the 36 summers in 1979–2014 (Fig. 3). Above 99% prior confidence level, the 8-21-day periodicity peak band is clearly identified, indicating that the quasi-biweekly band is the dominant period over this HW core region in summer.

Then we wonder how many HW events are associated with QBWO in the 36 summers. Two criteria are used to select the HW events that are related to the significant QBWO cases: (1) both the minimum amplitude in the dry phase and one of the maximum amplitudes in the wet phase exceed 0.8 standard deviations of the time series of area-averaged band-filtered rainfall; (2) an HW event occurs during the dry phase of QBWO. Since some HW events happened at the beginning of July or the end of August, we extended the time series from June 21 to September 6 in order to include the entire life cycles of the these QBWO cases. According to this criterion, 31 HW events associated with 32 significant QBWO cycles are selected among all 57 HW events, indicating that more than half of HW events are related to QBWO (Fig. 4). Therefore, we focused on the QBWO-associated HW events over YRV.

4 Common characteristics of local QBWO over YRV during HW events

To investigate what happens during the QBWO-associated HW events, we first examined the peak dry phase (phase 5) of a QBWO life cycle by phase composite analysis of all cases (Fig. 5). At the extreme dry phase, the most remarkable feature is a lower-tropospheric anticyclonic anomaly (LAA) over southeastern China, which corresponds to strong descending motions, suppressed rainfall and increasing temperature over YRV.

Why does the local temperature increases sharply at the dry phase of QBWO? The difference of QBWO-associated temperature between the extreme phases is 1.73 °C which accounts for nearly 80% to the total temperature difference that is 2.2 °C. This indicates that QBWO plays a

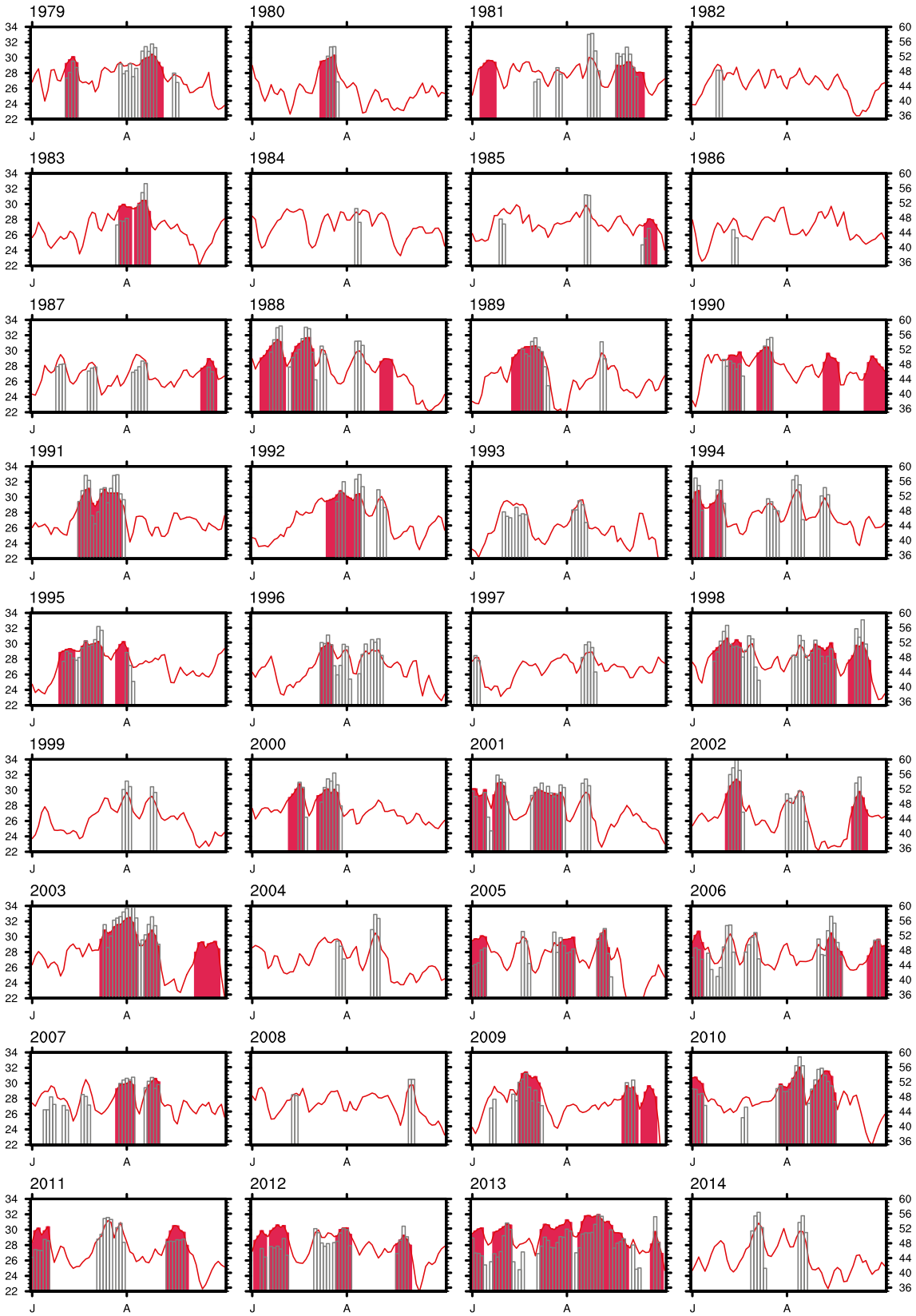

Fig. 2 Time series of YRV core region averaged T_m (*red solid line* and *red bar*, °C) with values in the *left y axis* and maximum HW index with values in the *right y axis* (*gray bar*) in each summer of 36 years. *Red bars* represent 63 HW events according to the relative definition and *gray bars* represent 111 HW events according to the absolute definition

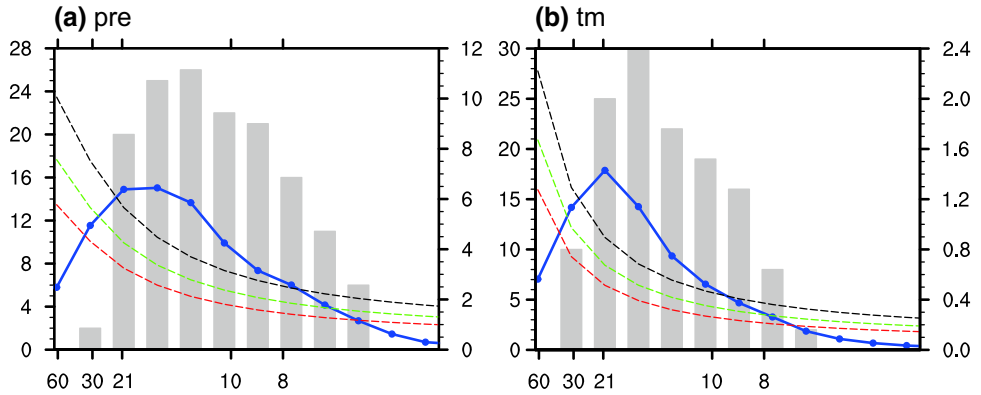

Fig. 3 36 summer mean power spectrum of the ISV component of daily **a** rainfall and **b** T_m over the YRV core region (*blue lines* with values in the *right y axis*), compared with Markov red noise spectra (*dashed red lines*), a priori 99% confidence bound (*dashed green lines*) and a posterior 99% confidence level (*dashed black lines*). The *grey bars* with values in the *left y axis* denote the frequency for each periodicity when its spectral power is significant at 99% confidence level

predominant role in generating the extremely high temperature during HW. To understand the physical process, the temperature budget equation in the lower troposphere and the associated evolutions of atmospheric vertical motion on the quasi-biweekly timescale over the YRV core region were diagnosed (Fig. 6). As a result, it is clear that the adiabatic process and diabatic process play the key role in heating the atmosphere from phase 3 till 5 with maximum heating rate of 0.21 K/day and 0.37 K/day, respectively, which is associated with the establishment of subsidence. In addition, the warm horizontal advection exhibits in the lower troposphere during the initiation period (before phase 2), which is only found in the HW events associated with "double wavetrains" QBWO (addressed in Sect. 5). Consequently, the maximum temperature appears after the extreme dry phase (at phase 6) since the temperature tendency is positive from phase 2 to 5, which proves that the local temperature increase is resulted from the atmospheric circulation.

Since the surface heat flux is an important component of atmospheric apparent heat source and has a considerable impact on the temperature near the surface, the QBWO-associated cloud cover and surface radiation fluxes were examined (Fig. 7). The core region averaged cloud cover is significantly reduced by 9% from phase 3 to 6 due to the LAA and its corresponding anomalous descending motions (Fig. 7a), which remarkably increases the surface downward shortwave radiation (Fig. 7b). Correspondingly, the surface upward sensible heat flux, latent heat flux and net longwave radiation flux are increased, which warm the atmosphere near the surface and generate HW events. The positive contribution of cloud and radiation to the HW events has also been emphasized in previous studies (e.g., Wu et al. 2012a, b).

5 Spatiotemporal evolutions of three types of QBWO associated with HW events over YRV

In the previous section, we showed that the extremely high temperature over YRV during HW was caused by the QBWO-associated local LAA with descending motion. To track where the LAA with subsidence originate, the evolutions of QBWO were explored by applying phase composite analysis for the 8-21-day filtered lower- and upper-tropospheric circulations during selected 31 HW events (figure not shown). The results indicate that QBWO over YRV might result from an eastward propagating wave train in the upper-troposphere from Western Europe to southeastern China roughly along the westerly jet and a northwestward migrating wave train from equatorial WNP to South China Sea. Then by using case-by-case analysis through 31 cases which has been used by previous studies (Wang and Rui 1990; Wang and Duan 2015), we found that although the LAA is a common feature, the upper-level circulation patterns and the associated wave trains are different during HW events (Fig. 8).

According to the distinct spatiotemporal features of QBWO which will be discussed later, 31 HW events are classified into three categories according to three criteria (Table 1): (1) If there is only an eastward propagating mid-latitude wave train in the upper troposphere in one case, this case will be identified as a HW event associated with "mid-latitude wavetrain" QBWO; (2) If there is only a northwestward propagating wave train over WNP in the lower troposphere or there is also an eastward propagating wave train in the upper troposphere but the upper-level geopotential height anomaly over YRV is greater than zero during the transition phase in one case, this case will be identified as a HW event associated with "WNP

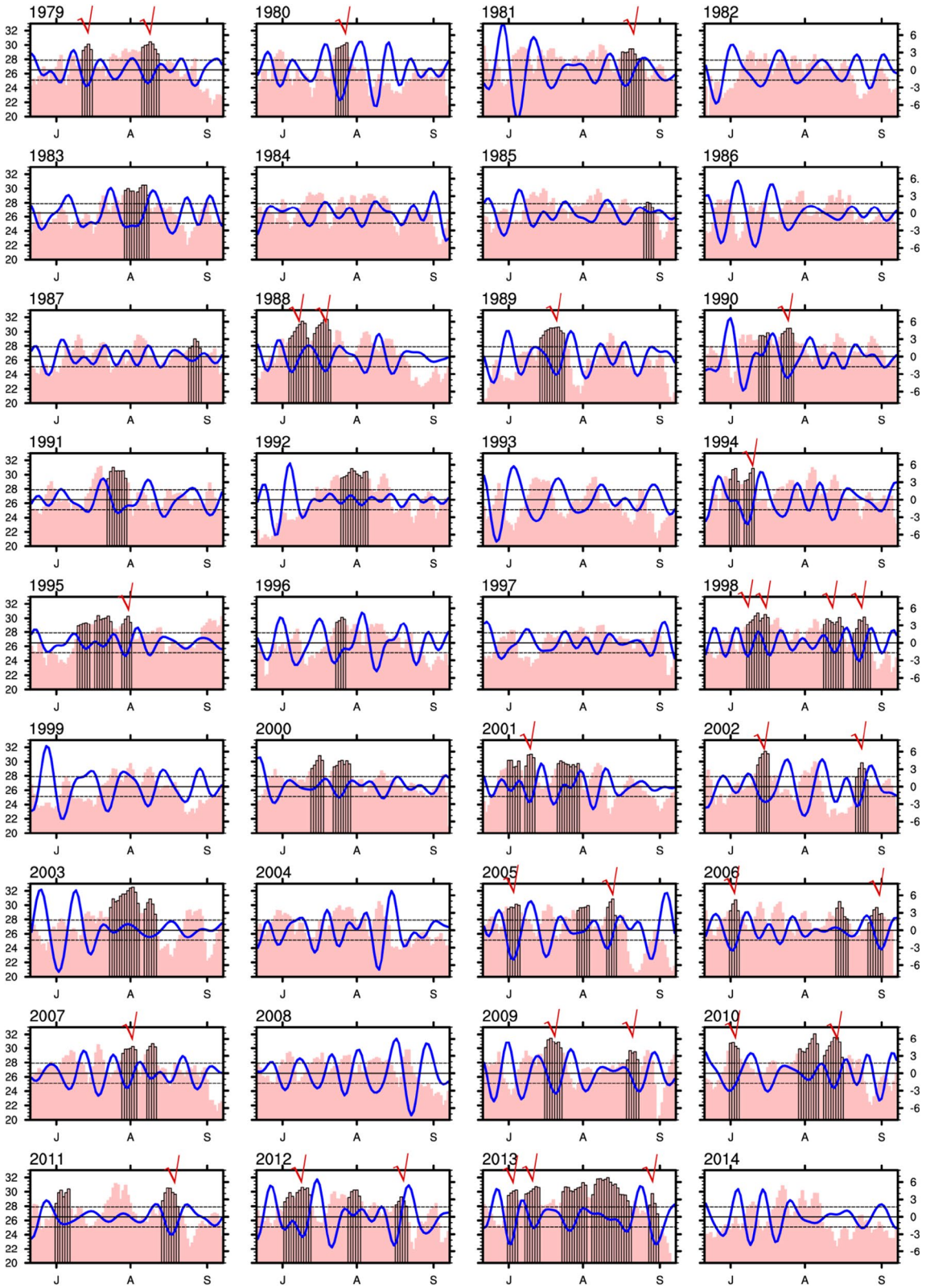

Fig. 4 Time series of unfiltered T_m (*red bar*, °C) with values in the *left y axis* and 8-21-day filtered precipitation (*blue solid line*, mm/day) with values in the *right y axis* averaged over the YRV core region during each summer of 36 years. *Black bars* denote the HW events. *Red ticks* represent 32 significant cases of QBWO related to HW events. *Dashed line* represents 0.8 standard deviation of precipitation

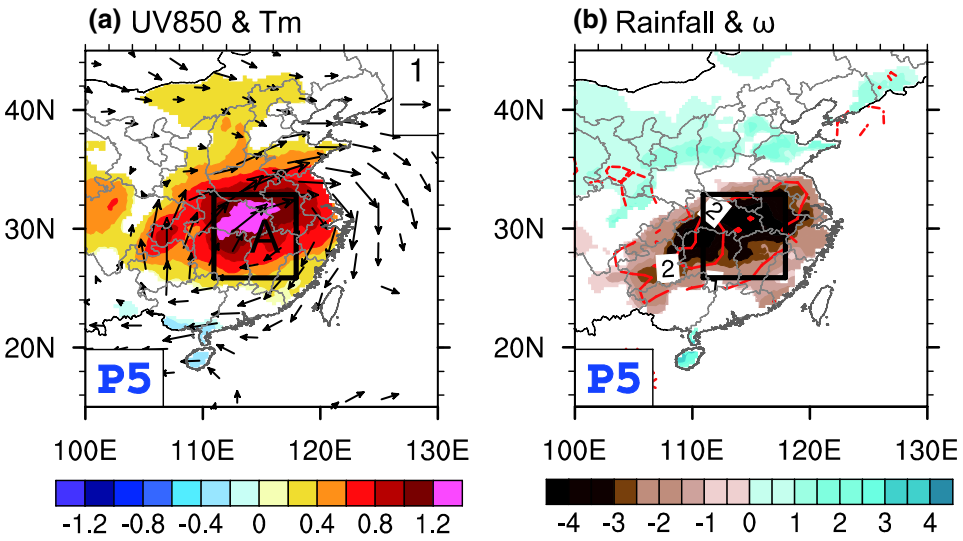

Fig. 5 8-21-day filtered **a** 850 hPa winds (*vector*: m/s), T_m (*shading*: °C), **b** weighted vertical velocity (contour: 10^{-2} Pa/s) and precipitation (*shading*: mm/day) at phase 5 based on the phase composite technique for 30 QBWO-associated HW events. Only the results significant at 90% confidence level are displayed. *Solid line* denotes positive value and *dashed line* denotes negative value. "*A*" denote the centers of anticyclonic anomaly. *Black box* is YRV core region. "*P*" means "phase"

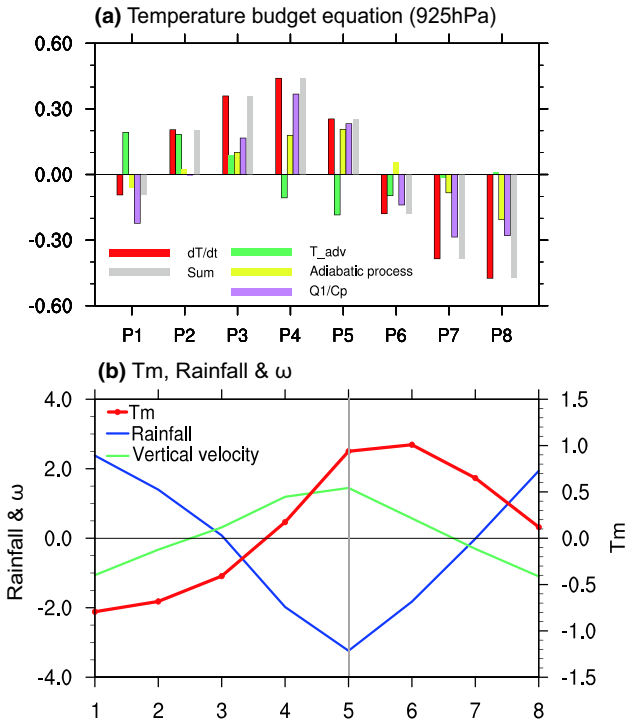

Fig. 6 **a** Temperature budget terms over YRV at 925 hPa during each phases of QBWO based on the phase composite technique for 30 HW events. From left to right: 8-21-day filtered temperature tendency (*red*), horizontal advection of temperature (*green*), adiabatic heating (*yellow*), diabatic heating (*purple*) and sum of three terms of heating (*grey*) (K/day). *Black boxes* denote the terms of the equation significant at 90% confidence level. **b** T_m (*red*: °C) with values in the *right y axis*, precipitation (*blue*: mm/day) and vertical velocity (*green*: 10^{-2} Pa/s) with values in the *left y axis* during each phases of QBWO over YRV based on the phase composite technique for 30 HW events

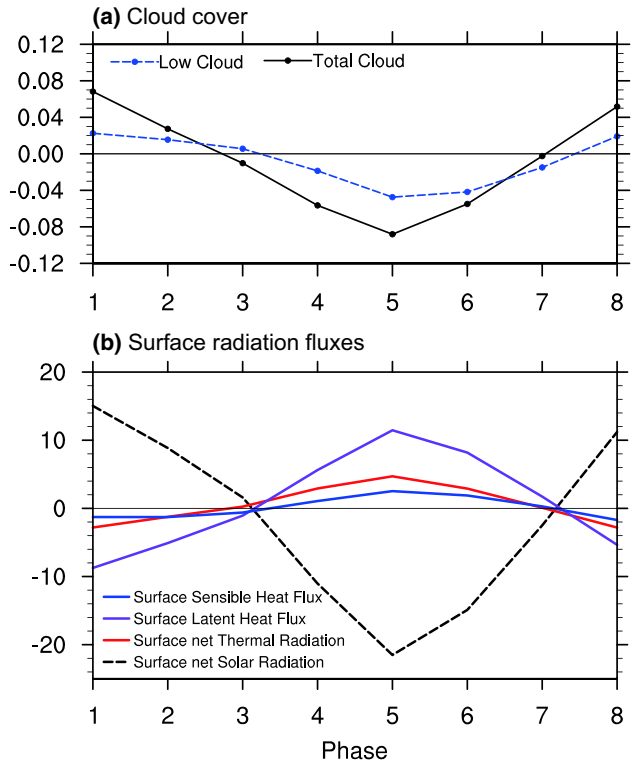

Fig. 7 Evolution of **a** cloud cover and **b** surface radiative fluxes (W/m^2, upward positive) over YRV based on the phase composite technique for 30 QBWO-associated HW events. **a** *Dashed blue line* is low cloud cover. *Black line* is total cloud cover. **b** *Dashed black line* is surface net solar radiation. *Red line* is surface net thermal radiation. *Purple line* is surface latent heat flux. *Blue line* is surface sensible heat flux

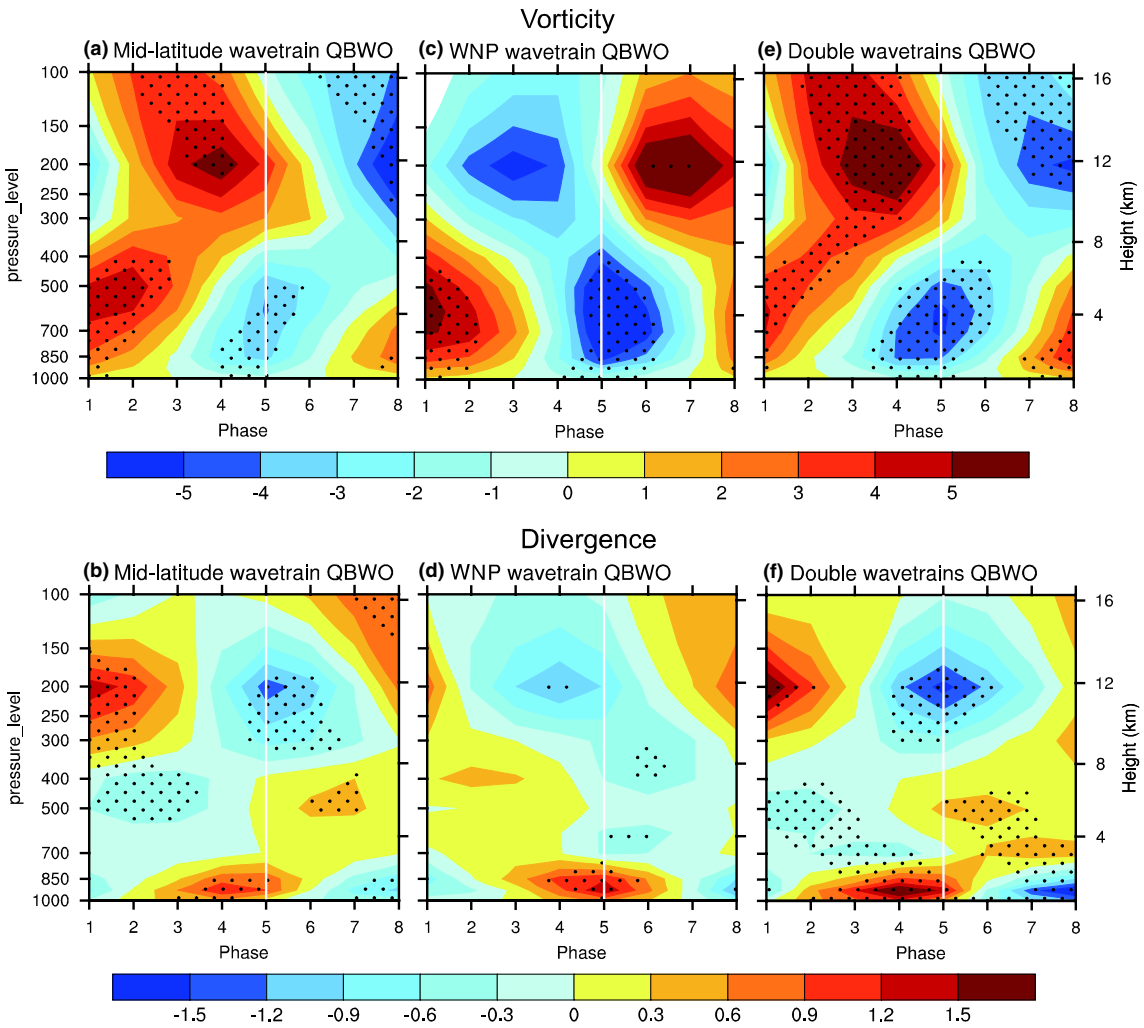

Fig. 8 8-21-day filtered **a, c, e** vorticity (10^{-6} s^{-1}) and **b, d, f** divergence (10^{-6} s^{-1}) at YRV during each phases of QBWO based on the phase composite technique for **a, b** 10 HW events associated with mid-latitude wavetrain QBWO, **c, d** 6 HW events associated with WNP wavetrain QBWO, **e, f** 14 HW events associated with double wavetrains QBWO, respectively. *Black dotes* denote the results significant at 90% confidence level

wavetrain" QBWO; (3) If there are both a northwestward propagating wave train over WNP in the lower troposphere and an eastward propagating mid-latitude wave train in the upper troposphere in one case, this case will be categorized into a HW event associated with "double wavetrains" QBWO. For simplicity, the first HW event in 1998 is regarded as 2 HW events induced by 2 significant QBWO cases. The HW events associated with QBWO from 1998-7-3 to 1998-7-11 and from 2013-6-26 to 2013-7-5 will not be discussed here because the atmospheric circulation doesn't show significant wave train features. Then the 8-phase composite technique was applied to the 8-21-day filtered fields for each type of QBWO-associated HW events respectively (Figs. 9, 10, 11). As we concentrated on the process of high temperature development, only the first half-life cycle from the peak wet phase (phase 1) to peak dry phase (phase 5) were depicted.

5.1 HW events associated with mid-latitude wavetrain QBWO

For the HW events associated with mid-latitude wavetrain QBWO, the LAA with subsidence over YRV are generated by an eastward/southeastward migratory wave train in the upper troposphere (Fig. 9b). The wave anomalies start from Eastern Europe, migrate through West Siberian Plain, Lake Baikal along the north edge of subtropical westerly jet, then propagate southeastward across the westerly jet, and reach southeastern China. After passing YRV, the wave train moves towards WNP. With the propagation of this wave train, during the developing phase (phase 2–4), take phase 3 for example, the centers of anticyclonic/cyclonic anomalies locate at the Arabian Peninsula, West Siberian Plain, Lake Baikal and southeastern China. The upper-tropospheric positive vorticity over the YRV core region which

Table 1 30 HW events associated with three types of QBWO with the begin and end dates (year-month-day) of each QBWO life cycle

HW associated with Mid-latitude wavetrain QBWO		HW associated with WNP wavetrain QBWO		HW associated with double wavetrains QBWO	
Phase 1	Phase 8	Phase 1	Phase 8	Phase 1	Phase 8
1979-8-1	1979-8-11	1988-6-30	1988-7-9	1979-7-8	1979-7-17
1998-7-12	1998-7-20	2002-7-8	2002-7-22	1980-7-18	1980-7-30
1998-8-8	1998-8-15	2005-8-4	2005-8-13	1981-8-11	1981-8-22
1998-8-17	1998-8-26	2006-8-25	2006-9-4	1988-7-12	1988-7-23
2005-6-27	2005-7-10	2009-8-16	2009-8-27	1989-7-12	1989-7-24
2010-6-21	2010-7-17	2012-8-10	2012-8-19	1990-7-18	1990-7-31
2010-8-7	2010-8-15			1994-7-3	1994-7-12
2012-7-5	2012-7-13			1995-7-24	1995-8-1
2013-6-26	2013-7-5			2001-7-5	2001-7-13
2013-8-23	2013-9-4			2002-8-17	2002-8-25
				2006-6-25	2006-7-6
				2007-7-24	2007-8-2
				2009-7-13	2009-7-24
				2011-8-10	2011-8-21

is associated with the cyclonic anomaly over southeastern China induces upper-level convergence, triggers descending motions and finally leads to the formation of low-level divergence and local LAA (Fig. 8a, b).

5.2 HW events associated with WNP wavetrain QBWO

In contrast, during the HW events associated with WNP wavetrain QBWO, LAA essentially comes from a northwestward migrating wave train over WNP in the lower troposphere (Fig. 10a). This northwest-southeast tilted wave train originates from tropical WNP (approximately 150°–170°E, 5°S to 10°N), passes over Philippine Sea, the East China Sea, Taiwan and moves toward southeastern China, which is consistent with the Rossby wave on the quasi-biweekly timescale proposed in previous studies (Yang and Wang 2008; Chen and Sui 2010). With the northwestward propagation of this low-level wave train, LAA directly moves into the YRV core region and induces local divergence and subsidence (Fig. 8c, d).

5.3 HW events associated with double wavetrains QBWO

For HW events associated with double wavetrains QBWO, the LAA with subsidence over YRV are triggered by the superimposed effect of two wave trains in both of the lower and upper troposphere (Fig. 11). In the lower troposphere, the most remarkable characteristic is a northwestward/westward propagating wave train extending from tropical WNP to South China Sea (Fig. 11a). In contrast to the low-level wave train in HW events associated with WNP wavetrain QBWO, this wave train originates from tropical WNP (approximately 155°–170°E, 5°S to 10°N), propagates southwestward through Philippine Sea, and then moves westward to South China Sea (Kikuchi and Wang 2009).

In the upper troposphere, a notable mid-latitude "Silk Road pattern"-like wave train (Enomoto et al. 2003) is clearly seen starting from Eastern Europe, passing the Lake Balkhash and then propagating eastward roughly along the subtropical westerly jet (Fig. 11b). When this wave train reaches the northeast of Tibetan Plateau, it turns along the streamflow of South Asian High in a clockwise direction and crosses the YRV core region, which is consistent with the wave train on the quasi-biweekly timescale described by Yang et al. (2016).

On one hand, with the northwestward/westward migration of the low-level wave train, the centers of anticyclonic/cyclonic anomalies appear over Melanesia Basin, Caroline Islands and South China Sea during the developing phase. The easterly wind anomalies associated with the cyclonic anomaly over South China Sea provides an anti-cyclonic shear vorticity to the core region (Fig. 8e). On the other hand, with the eastward/southeastward propagation of upper-level wave train, the centers of the wave train locate at Eastern Europe, Tian Shan, the Qilian Mountains and southeastern China during the developing phase. Correspondingly, the cyclonic anomaly over southeastern China induces upper-level positive vorticity with convergence over YRV. Thus, a vertical baroclinic structure which has upper-level cyclonic vorticity with convergence and low-level anti-cyclonic vorticity with divergence over the core region contributes to the local descending motion and the formation of LAA (Fig. 8e, f).

According to Figs. 9, 10 and 11, we also noticed an evident opposite movement of the WNPSH and South Asian High in all HW events, i.e., WNPSH extends westward (eastward) while South Asian High extends eastward (westward) respectively at the extreme dry (wet)

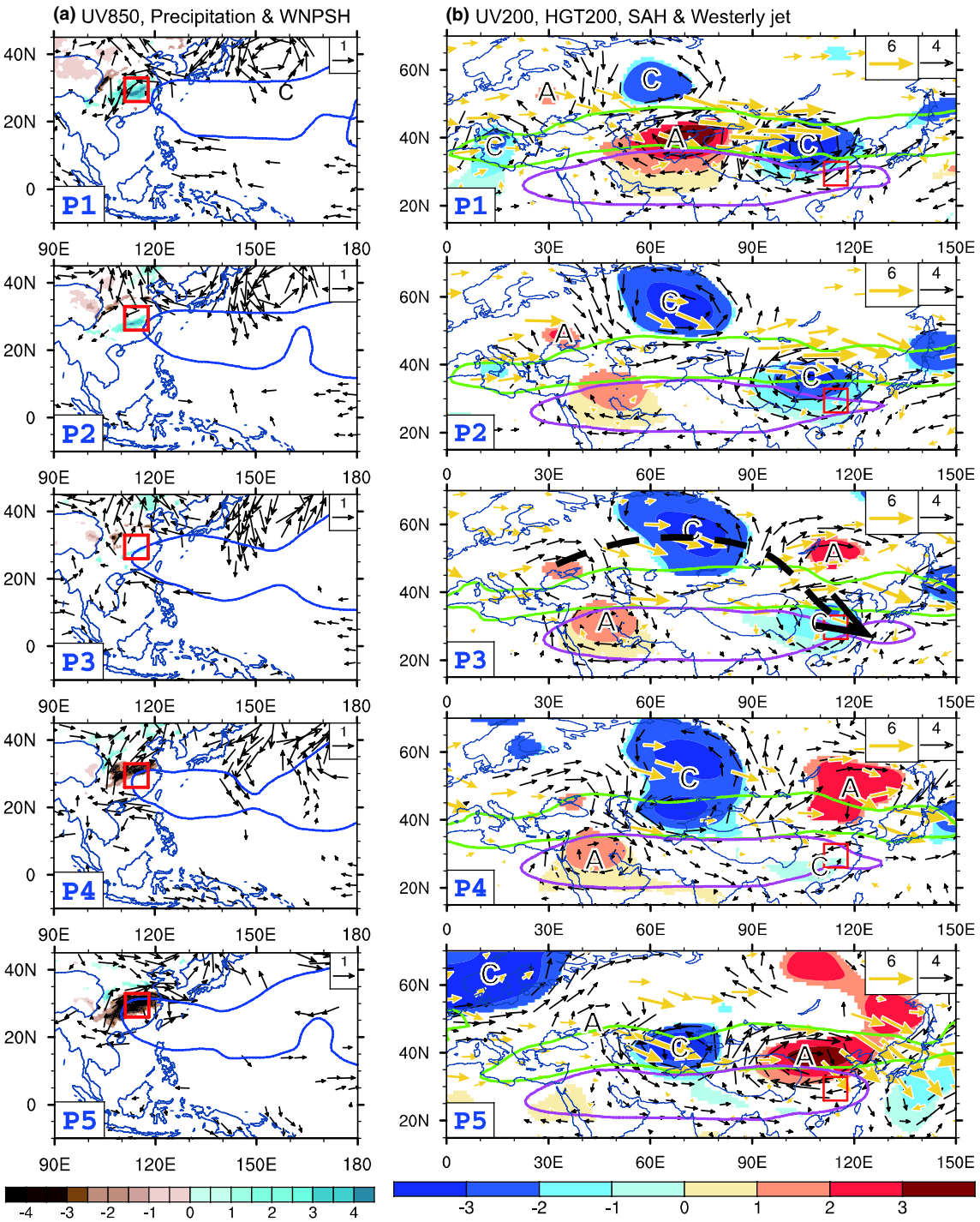

Fig. 9 Temporal evolution of **a** 850 hPa winds (*vectors*: m/s), precipitation (*shadings*: mm/day), **b** 200 hPa winds (*black vectors*: m/s), geopotential height (*shading*: 10gpm) and wave-activity flux (*yellow vectors*, m^2/s^2) on the 8-21-day timescale based on phase composite technique for 10 HW events associated with mid-latitude wave-train QBWO. Only the results significant at 90% confidence level are shown. *Red box* is the YRV core region. *Blue lines* in the *left panel* are 850 hPa geopotential height contours by the 588 10 gpm that roughly represent the WNPSH location. *Green lines* in the *right panel* are zonal wind contours by 20 m/s that roughly denote the location of subtropical westerly jet. *Pink lines* in the *right panel* are 200 hPa geopotential height contours by the 1254 10 gpm that roughly represent the South Asian High location. "*C*" and "*A*" denote the center of the cyclonic and anti-cyclonic anomaly, respectively. *Dashed balck arrows* indicate the track of the propagation of wave trains. "*P*" means "phase"

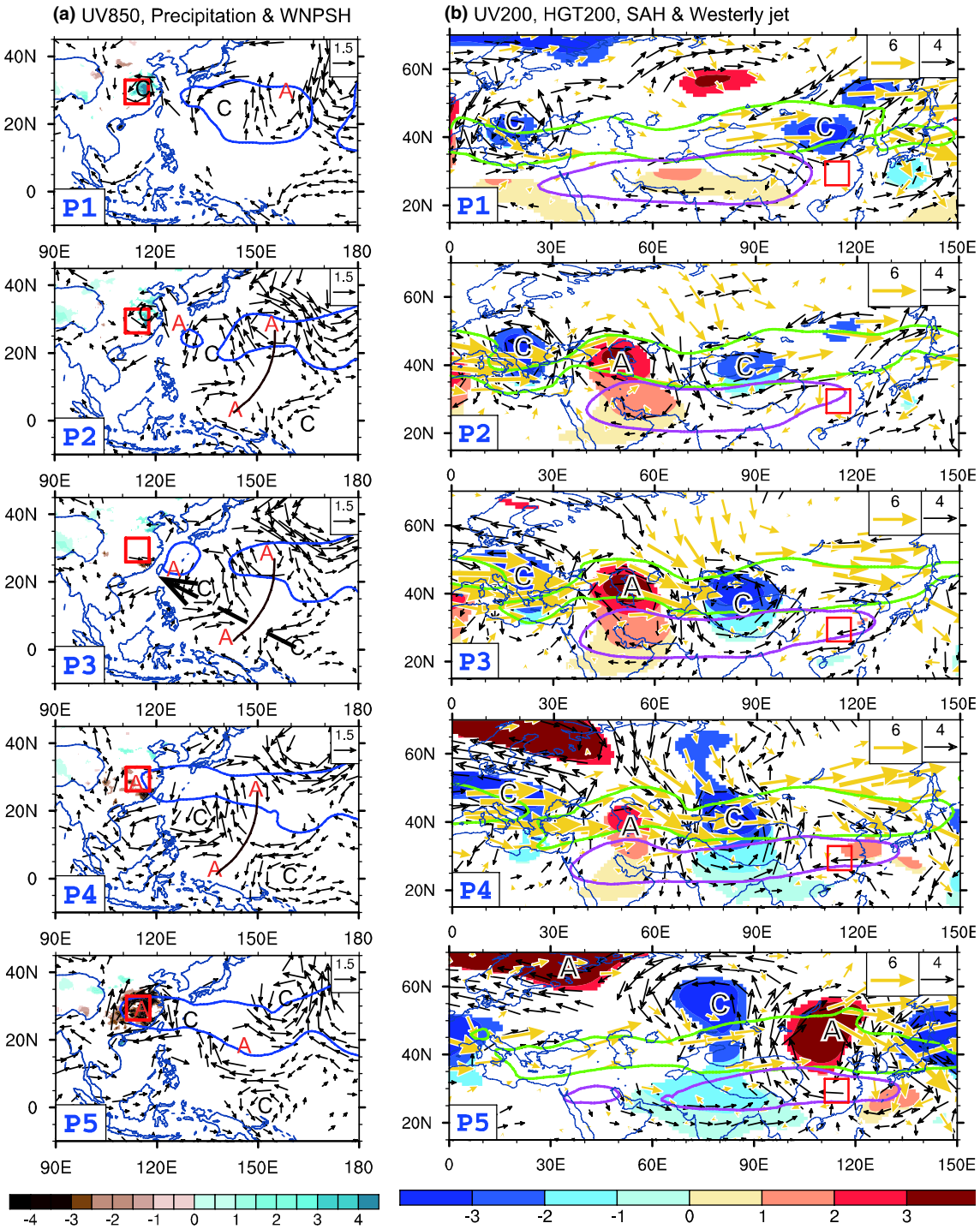

Fig. 10 Same as Fig. 9, except for the composite for 6 HW events associate with WNP wavetrain QBWO

phase. The "face-to-face" displacement of two large-scale systems during the QBWO developing phase is resulted from the formation of LAA over YRV and the mid-latitude wave train. This movement of South Asian High and WNPSH in summer has also been proposed by previous studies on the quasi-biweekly timescale (e.g., Jia and Yang 2013; Yang et al. 2014), which is favorable for the HW occurrence in China (Liu et al. 2006; Peng 2014).

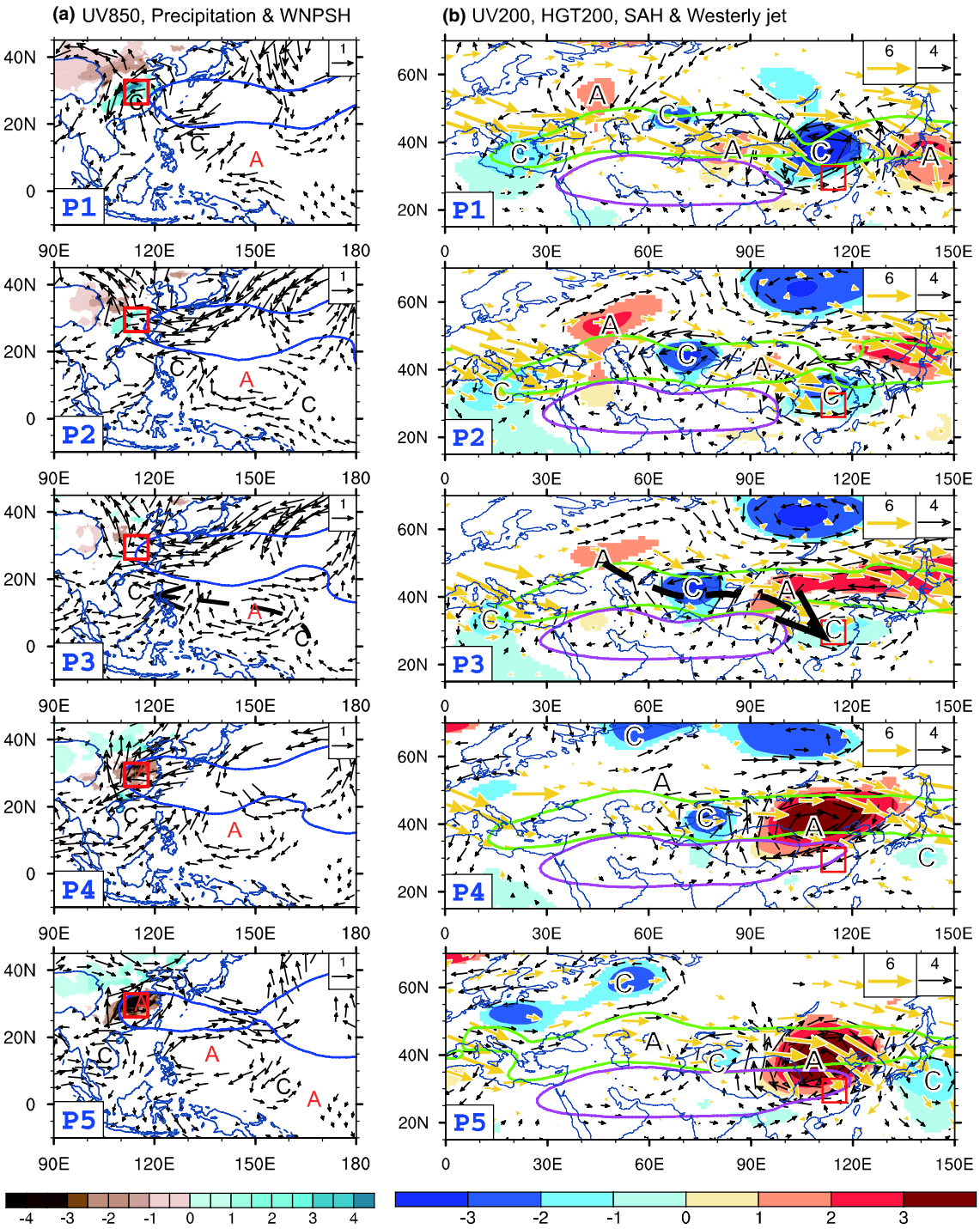

Fig. 11 Same as Fig. 9, except for the composite for 14 HW events associate with double wavetrains QBWO

6 Conclusion and discussion

6.1 Conclusion

This study found 55% of HW events (30/57) over YRV are associated with the atmospheric QBWO (8-21-day) in JA during the period from 1979 to 2014. QBWO component accounts for nearly 80% to the temperature increase. The key linkage between QBWO and HW events is a LAA over the core region, accompanied with local strong subsidence which causes extremely high temperature through increasing adiabatic heating and downward shortwave radiation.

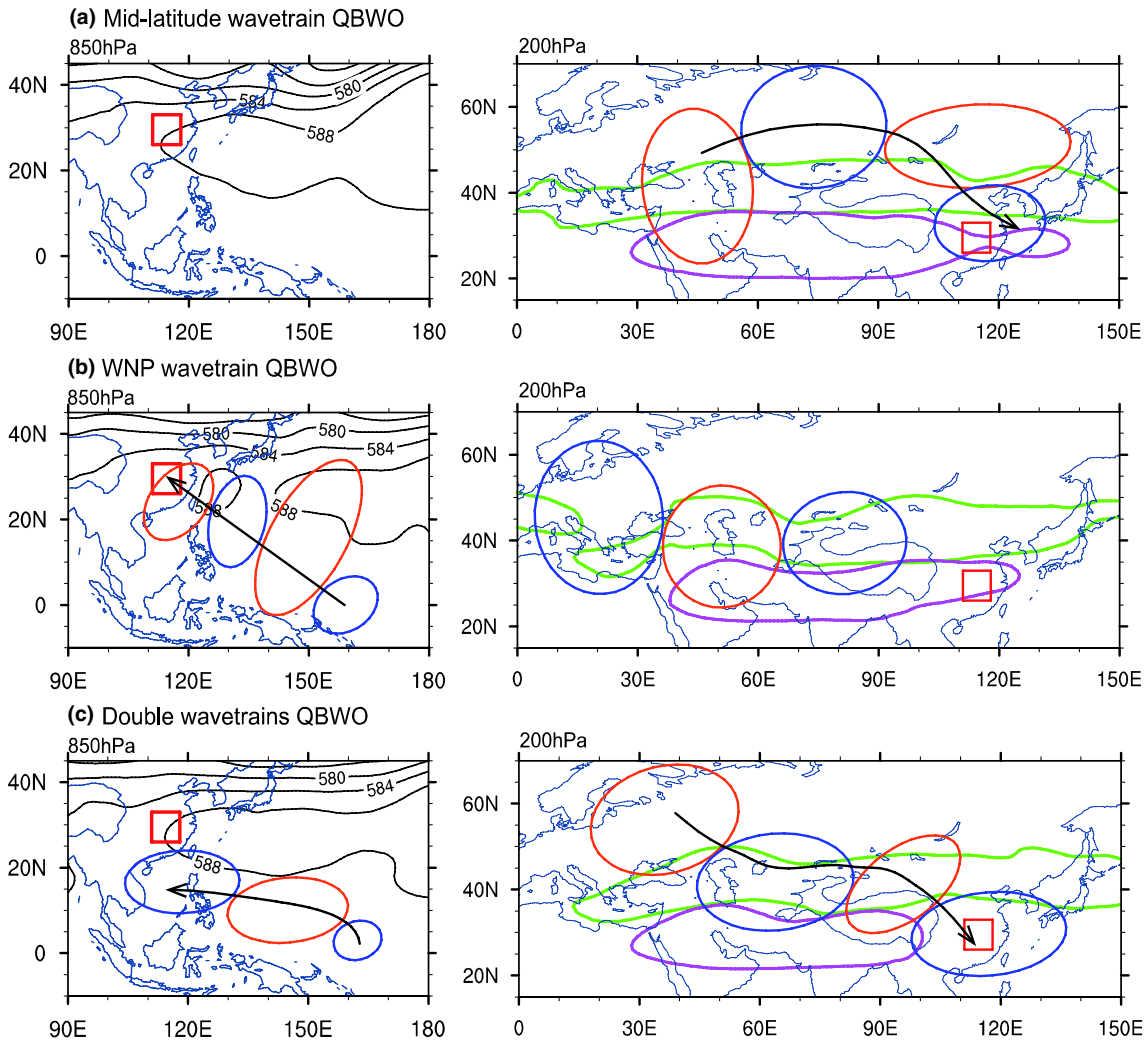

Fig. 12 Schematic diagram of the propagation of lower-level and mid-latitude upper-level wave trains based on phase 3 of QBWO in HW events associated with **a** mid-latitude wavetrain, **b** WNP wavetrain and **c** double wavetrains QBWO, respectively. The *blue* and *orange circles* represent the cyclonic and anticyclonic anomalies, respectively. *Black lines* in the left panel are 850 geopotential height (10 gpm). *Green lines* in the *right panel* are zonal wind contours by 20 m/s that roughly denote the location of subtropical westerly jet. *Pink lines* in the *right panel* are 200-hPa geopotential height contours by the 1254 10 gpm that roughly represent the South Asian High location. *Black arrows* indicate the track of the propagation of wave trains

The local LAA genesis is associated with three types of QBWO wave trains, named as "mid-latitude wavetrain", "WNP wavetrain" and "double wavetrains", respectively. As we summarized in the schematic diagram (Fig. 12), mid-latitude wavetrian QBWO features an eastward/southeastward migratory wave train propagating along the north edge of the westerly jet from Eastern Europe to WNP in the upper troposphere. WNP wavetrain QBWO is dominated by a clear northwestward propagating low-level wave train from tropical WNP to southeastern China. Double wavetrains QBWO is characterized by both an upper-level eastward/southeastward propagating wave train roughly along the subtropical westerly jet from Eastern Europe to southeastern China and a low-level northwestward/westward migrating wave train propagating from tropical WNP to the South China Sea.

In detail, mid-latitude wavetrain QBWO generates the LAA primarily through the local subsidence forced by the upper-level positive vorticity with convergence. WNP wavetrain QBWO causes the LAA by the northwestern propagation of the low-level wave train. Double wavetrains QBWO forms LAA through both subsidence triggered by upper-level cyclonic vorticity with convergence and low-level anticyclonic shear vorticity.

Through case-by-case categorization and composite analysis, this study interprets the genesis processes of most HW events over YRV by linking them with

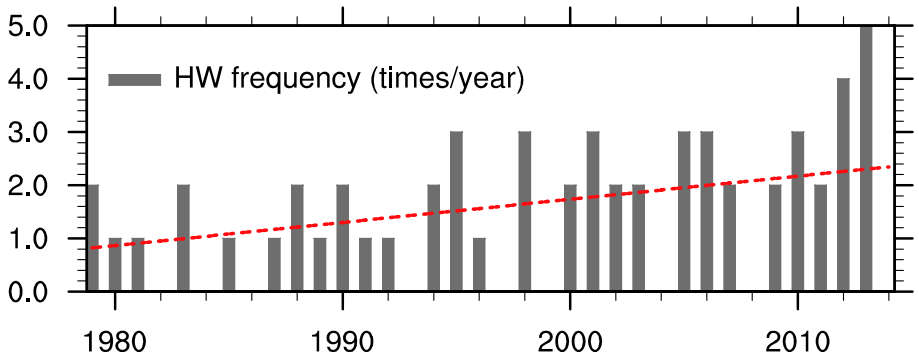

Fig. 13 The year to year variation (*gray bar*: times/year) and trend (*red line*: times/year) of HW frequency over the YRV core region in JA during 1979–2014

atmospheric QBWO, which facilitate the better understanding of HW occurrence over YRV.

6.2 Discussion

We only explained 55% of HW events over YRV through QBWO. How about the other 27 HW events? We noticed that these HW events might relate to atmospheric variation with longer periodicity than biweekly. Through power spectrum and band-filtered analysis based on the datasets covering boreal summer (May–October), we found 8 HW events among them [1990(1st), 1996, 1998(1st), 2001(3rd), 2003(1st), 2012(2nd), 2013(2nd) and 2013(3rd)] are related to the significant atmospheric 21-26-day variation. And 10 HW events [1983, 1991, 1992, 1996, 2003(1st), 2003(2nd), 2010(2nd), 2012(2nd), 2013(3rd) and 2013(4th)] occurred near August 1st are likely associated with quasi-60-day variation, which may belong to part of the climatological intraseasonal oscillation (CISO) (Wang and Xu 1997). We will investigate them in our next work.

In terms of HW frequency, we found an interesting phenomenon using the Mann–Kendall non-parametric test. The annual HW occurrence over YRV shows significant positive trend with a magnitude of 0.43 times/decade during the past 36 years (Fig. 13), which is consistent with previous studies (e.g., Ye et al. 2014; Ding and Ke 2015). Whether it has relationship with decadal variation of ISV is worthwhile to be further examined.

The finding about close relationship between HW events over YRV and QBWO in this study aims to improve HW prediction. Based on more HW in longer record datasets, we are calculating the probability of HW occurrence with the appearance of atmospheric anomalies at the developing phase of QBWO in our ongoing study.

Acknowledgements This study was supported by funds from the National Key Research and Development Program–Global Change and Mitigation Project: Global change risk of population and economic system: mechanism and assessment (Grant No. 2016YFA0602401), the National Natural Science Foundation of China (Grant No. 41375003, Grant No. 41621061 and Grant No. 41420104002) and the project PE16010 of the Korea Polar Research Institute. BW acknowledges the support from Climate Dynamics Program of the National Science Foundation under award No AGS-1540783, NOAA/DYNAMO #NA13OAR4310167 and the National Research Foundation (NRF) of Korea through a Global Research Laboratory (GRL) Grant (MEST, #2011–0021927). This is the ESMC publication number 145.

References

Anderson GB, Bell ML (2011) Heat waves in the United States: mortality risk during heat waves and effect modification by heat wave characteristics in 43 U.S. Communities. Environ Heal Perspect 119:210–218

Bingham C, Godfrey MD, Tukey JW (1967) Modern techniques of power spectrum estimation. IEEE Trans Audio Electroacous 15 (2):6–66

Bloomfield P (2000) Fourier analysis of time series: an introduction, 2nd edn. Wiley, Hoboken, NJ

Chan JCL, Ai W, Xu J (2002) Mechanisms responsible for the maintenance of the 1998 South China Sea summer monsoon. J Meteorol Soc Jpn 80(5):1103–1113

Chen GH, Sui CH (2010) Characteristics and origin of quasi-biweekly oscillation over the western North Pacific during boreal summer. J Geophys Res Atmos 115 (D14113). doi:10.1029/2009JD013389

Chen JP, Wen ZP, Wu RG, Chen ZS, Zhao P (2015) Influences of northward propagating 25-90-day and quasi-biweekly oscillations on eastern China summer rainfall. Clim Dyn 45:105–124

Dee DP, Uppala SM, Simmons AJ et al (2011) The ERA-Interim reanalysis: configuration and performance of the data assimilation system. Q J Roy MeteorSoc 137(656):553–597

Ding T, Ke ZJ (2015) Characteristics and changes of regional wet and dry heat wave events in China during 1960–2013. Theor Appl Climato 122(3):651–665

Ding T, Qian WH (2011) Geographical patterns and temporal variations of regional dry and wet heatwave events in China during 1960–2008. Adv Atmos Sci 28(2):322–337

Ding T, Qian WH (2012) Statistical characteristics of heat wave precursors in China and model prediction. Chin J Geophys 55 (5):1472–1486 (**in Chinese**)

Easterling DR, Meehl GA, Parmesan C, Changnon SA, Karl TR, Mearns LO (2000) Climate extremes: observations, modeling, and impacts. Science 289(5487):2068–2074

Enomoto T, Hoskins BJ, Matsuda Y (2003) The formation mechanism of the Bonin high in August. Q J Roy Meteorol Soc 129:157–178

Fujinami H, Yasunari T (2004) Submonthly variability of convection and circulation over and around the Tibetan Plateau during the boreal summer. J Meteorol Soc Jpn 82(6):1545–1564

Gershunov A, Cayan DR, Iacobellis SF (2009) The great 2006 heat wave over California and Nevada: Signal of an Increasing Trend. J Clim 22:6181–6203

Gilbert RO (1987) Statistical methods for environmental pollution monitoring. Wiley, New York, pp 217–219

Gilman DL, Fuglister FJ, Mitchell JM Jr (1963) On the power spectrum of red noise. J Atmos Sci 20(2):182–184

Gong DY, Pan YZ, Wang JA (2004) Changes in extreme daily mean temperatures in summer in eastern China during 1955–2000. Theor Appl Climato 77 (1):25–37

Hartmann DL, Klein Tank AMG, Rusticucci M, Alexander LV, Brönnimann S, Charabi Y, Dentener FJ, Dlugokencky EJ, Easterling DR, Kaplan A, Soden BJ, Thorne PW, Wild M, Zhai PM (2013) Observations: atmosphere and surface. In: Stocker TF, Qin D, Plattner G-K, Tignor M, Allen SK, Boschung J, Nauels A, Xia Y, Bex V, Midgley PM (eds) Climate change 2013: the physical science basis. Contribution of working group I to the fifth assessment report of the intergovernmental panel on climate change. Cambridge University Press, Cambridge and New York, pp 159-254

Hu KM, Huang G, Qu X, Huang RH (2012) The impact of Indian Ocean variability on high temperature extremes across the southern Yangtze River valley in late summer. Adv Atmos Sci 29 (1):91–100

Huang W, Kan HD, Kovats S (2010) The impact of the 2003 heat wave on mortality in Shanghai, China. Sci Total Environ 408(11):2418–2420

Jia XL, Yang S (2013) Impact of the quasi-biweekly oscillation over the western North Pacific on East Asian subtropical monsoon during early summer. J Geophys Res Atmos 118(10):4421–4434

Kendall MG (1975) Rank correlation methods, 4th edn. Charles Griffin, London

Kikuchi K, Wang B (2009) Global perspective of the quasi-biweekly oscillation. J Clim 22(6):1340–1359

Lei YN, Gong DY, Zhang ZY, Guo D, He XZ (2009) Spatial-temporal characteristics of high-temperature events in summer in eastern China and the associated atmospheric circulation. Geogr Res 28(3):653–662 (**in Chinese**)

Levy R, Hsu C et al (2015) MODIS atmosphere L2 aerosol product. NASA MODIS adaptive processing system, Goddard space flight center. (Terra, USA. 10.5067/MODIS/MYD04_L2.006 (**Aqua**)

Liu HZ, Zhao SR, Zhao CG, Lu ZS (2006) Weather abnormal and evolutions of western Pacific subtropical high and South Asian High in summer of 2003. Plateau Meteor 25(2):169–178 (**in Chinese**)

Liu LL, Sun LH, Liao YM, Zhu YF, Zou XK, Wang YM, Yan JH (2008) Development and application of national prediction system for extreme high temperature. Meteorol Mon 34:102–107 (**in Chinese**)

Liu HB, Yang J, Zhang DL, Wang B (2014) Roles of synoptic to quasi-biweekly disturbances in generating the summer 2003 heavy rainfall in East China. Mon Weather Rev 142(2):886–904

Mao JY, Wu GX (2006) Intraseasonal variations of the Yangtze rainfall and its related atmospheric circulation features during the 1991 summer. Clim Dyn 27 (7):815–830

Meehl GA, Tebaldi C (2004) More intense, more frequent, and longer lasting heat waves in the 21st century. Science 305(5686):994–997

Peng J (2014) An investigation of the formation of the heat wave in southern China in summer 2013 and the relevant abnormal subtropical high activities. Atmos Oceanic Sci Lett 7 (4):286–290

Qian WH, Lin X (2004) Regional trends in recent temperature indices in China. Clim Res 27 (2):119–134

Robinson PJ (2001) On the definition of a heat wave. J Appl Meteor 40(4):762–775

Smith TT, Zaitchik BF, Gohlke JM (2013) Heat waves in the United States: definitions, patterns and trends. Clim chan 118(3):811–825

Steadman RG (1984) A universal scale of apparent temperature. J Clim Appl Meteorol 23:1674–1687

Sun JQ (2012) Possible impact of the summer North Atlantic oscillation on extreme hot events in China. Atmos Oceanic Sci Lett 5(3):231–234

Sun JQ (2014) Record-breaking SST over mid-North Atlantic and extreme high temperature over the Jianghuai-Jiangnan region of China in 2013. Chin Sci Bull 59:3465–3470

Takaya K, Nakamura H (2001) A formulation of a phase-independent wave-activity flux for stationary and migratory quasigeostrophic eddies on a zonally varying basic flow. J Atmos Sci 58:608–627

Teng HY, Branstator G, Wang H, Meehl GA, Washington WM (2013) Probability of US heat waves affected by a subseasonal planetary wave pattern. Nature Geosci 6(12):1056–1061

Wang MR, Duan A (2015) Quasi-biweekly oscillation over the Tibetan plateau and its link with the Asian Summer monsoon. J Clim 28:4921–4940

Wang B, Rui HL (1990) Synoptic climatology of transient tropical intraseasonal convection anomalies. Meteor Atmos Phys 44(1–4):43–61

Wang B, Xu XH (1997) Northern hemisphere summer monsoon singularities and climatological intraseasonal oscillation. J Clim 10(5):1071–1085

Wang B, Liu J, Yang J, Zhou TJ, Wu ZW (2009) Distinct principal modes of early and late summer rainfall anomalies in East Asia. J Clim 22(13):3864–3875

Wu J, Gao XJ (2013) A gridded daily observation dataset over China region and comparison with the other datasets. Chin J Geophys 56(4):1102–1111 (**in Chinese**)

Wu ZW, Lin H, Li JP, Jiang ZH, Ma TT (2012a) Heat wave frequency variability over North America: two distinct leading modes. J Geophys Res Atmos 117 (D02102). doi:10.1029/2011JD016908

Wu ZW, Jiang ZH, Li JP, Zhong SS, Wang LJ (2012b) Possible association of the western Tibetan Plateau snow cover with the decadal to interdecadal variations of northern China heatwave frequency. Clim Dyn 39 (9):2393–2402

Xu Y, Gao XJ, Shen Y, Xu CH, Shi Y, Giorgi F (2009) A daily temperature dataset over China and its application in validating a RCM simulation. Adv Atmos Sci 26(4):763–772

Yanai M, Esbensen S, Chu JH (1973) Determination of bulk properties of tropical cloud clusters from large-scale heat and moisture budgets. J Atmos Sci 30(4):611–627

Yang SY, Li T (2016) Intraseasonal variability of air temperature over the mid-high latitude Eurasia in boreal winter. Clim Dyn 47:2155–2175

Yang J, Wang B (2008) Anticorrelated intensity change of the quasi-biweekly and 30-50-day oscillations over the South China Sea. Geophys Res Lett 35(L16702). doi:10.1029/2008GL034449

Yang J, Wang B, Bao Q (2010) Biweekly and 21–30 day variabilities of the subtropical East Asian monsoon over the lower reach of Yangtze River Basin. J Clim 23(5):1146–1159

Yang J, Bao Q, Wang B, Gong DY, He HZ, Gao MN (2014) Distinct quasi-biweekly features of the subtropical East Asian monsoon during early and late summers. Clim Dyn 42 (5):1469–1486

Yang J, Bao Q, Wang B, He HZ, Gao MN, Gong DY (2016) Characterizing two types of transient intraseasonal oscillations in the Eastern Tibetan Plateau summer rainfall. Clim Dyn. doi:10.1007/s00382-016-3170-z

Ye DX, Yin JF, Chen ZH, Zheng YF, Wu RJ (2014) Spatial and temporal variations of heat waves in China from 1961 to 2010. Adv Clim Change Res 5 (2):66–73

Zhang RP, Zhou YF, Guo KY (2005) The relation between the persistent high temperature in south of China in the summer of 2003 and the vortex's position. Sci Meteorol Sin 25(5):528–533 (**in Chinese**)

Zhao CB, Li T, Zhou TJ (2013) Precursor signals and processes associated with MJO initiation over the tropical Indian Ocean. J Clim 26(1):291–307